A sequential sampling-based Bayesian numerical method for reliability-based design optimization

Fangqi Hong[a], Pengfei Wei[a,*], Jiangfeng Fu[a], Michael Beer[b,c,d]

[a]*School of Power and Energy, Northwestern Polytechnical University, Xi'an 710072, China*
[b]*Institute for Risk and Reliability, Leibniz Universität Hannover, Hannover 30167, Germany*
[c]*Institute for Risk and Uncertainty, University of Liverpool, Liverpool L69 7ZF, UK*
[d]*International Joint Research Center for Engineering Reliability and Stochastic Mechanics, Tongji University, Shanghai 200092, China*

Abstract

For efficiently solving the Reliability-Based Design Optimization (RBDO) problem with multi-modal, highly nonlinear and expensive-to-evaluate limit state functions (LSFs), a sequential sampling-based Bayesian active learning method is developed in this work. The penalty function method is embedded to transform the constrained optimization problem into a non-constrained one to reduce the model complexity. The proposed method for solving RBDO problems starts by training a Gaussian process (GP) model, in the augmented space of random and design variables. It is then based on an efficient sampling scheme for simulating the GP model, the adaptive Bayesian optimization (BO) and Bayesian reliability analysis (BRA) procedures are combined in a collaborative way for sequentially producing the joint training points. BO driven by expected improvement (EI) function is used for inferring the global optimum in the design space with global convergence, and the BRA equipped with U function is implemented for inferring the failure probabilities at the identified design points with the desired accuracy. The superiority of the proposed method is demonstrated with two numerical and two real-world engineering examples.

Keywords: Reliability-based design optimization; Bayesian optimization; Bayesian reliability analysis; Acquisition function; Gaussian process simulation

1. Introduction

Design optimization has been widely recognized as a cost-effective design technique of achieving high performance and reliability with low cost in mechanical engineering, aerospace engineering and civil engineering, etc. Uncertainties are iniquitous during different stages of product development, and failing to incorporate these uncertainties may result in misleading design configurations [1], this has highlighted the necessity of developing uncertainty-based design optimization methods. The uncertainty-based design optimization problems can be grouped into three types i.e., Reliability-Based Design Optimization (RBDO) [2], Robust Design Optimization [3] and Expected Life-cycle Cost Optimization [4]. One of the common challenges for all the above three types of optimization problems is the nested numerical trap, which means the necessity of optimizing the design parameters in the outer loop, and probabilistic analysis on (a set of)

*Corresponding author at School of Power and Energy, Northwestern Polytechnical University, Xi'an 710072, China
Email address: pengfeiwei@nwpu.edu.cn (Pengfei Wei)

expensive-to-evaluate simulators in the inner loop. The aim of this work is then to develop a numerically efficient method for addressing the above challenge, and specifically we focus on the RBDO problem.

For a typical RBDO problem, the available methods can be organized into three groups: approximate reliability methods, advanced Monte Carlo simulation, and surrogate model methods mostly equipped with active learning schemes. All these methods have been extended for addressing the RBDO problems in a double-loop or a single-loop or a decoupling scheme [5]. The approximate reliability methods are mostly based on searching the Most Probable Point (MPP) of the random variables, which is defined as the point having the highest probability density value within the failure domain, and typical methods include the First and Second Order Reliability Methods (FORM and SORM, respectively) [6]. Combined with a double-loop searching scheme, the FORM method has been extended, and named as Performance Measure Approach (PMA) for solving the RBDO problem [7]. For bypassing the time-consuming double loop, several single-loop schemes combined with FORM/SORM has been developed using e.g., the Karush–Kuhn–Tucker (KKT) optimality conditions [8]. The decoupling approaches driven by FORM/SORM are based on construction of approximate functional relationship between the reliability index and the design variables (see the Sequential Optimization and Reliability Assessment (SORA) as an example [9]). Overall, the FORM/SORM based methods are computationally efficient, but may lack suitability for problems with high-nonlinear constraints and multi-modal objectives/constraints.

Monte Carlo simulation (MCS), and its extensions, including importance sampling (see e.g., [10]), subset simulation [11], line sampling [12] and directional (importance) sampling [13], are versatile approaches for estimating the failure probability as there is a theoretical guarantee of convergence. Plenty of this group of methods have been extended for RBBO, most of which follow a decoupling scheme. For example, with the assumption that probability distribution of the random variables depend on the design variables, the subset simulation approach is copied with the augmented space perspective for estimating the reliability-based design sensitivity with only one simulation run [14]. This strategy is then extended, based on a weighting scheme, by using other advanced MCS methods such as line sampling [15] and subset simulation [16], for directly estimating the function of the failure probability over the design variables the bridge importance sampling has also been extended, by reusing the samples, for addressing RBBO [17]. In all, the decoupling strategies based on advanced MCS approaches are more suitable for high-nonlinear problems, but may lack accuracy efficiency due to the extensive numbers of required samples for convergence.

Motivated by the fast computation requirement for real-world engineering applications, the surrogate model approaches, especially the Gaussian Process Regression (GPR, or called Kriging) equipped with active learning, have received the most attention during the decades for RBDO [5]. For examples, for obtaining the accurate MPPs of the single loop approaches, the enhanced chaos control methods [18] and the most probable learning function [19] are developed for updating the GPR models of LSFs. In [20], the importance boundary sampling strengthened by the probability feasible region is developed to improve the computational efficiency of RBDO. In [21], the Kriging model is updated by the MPPs generated from the last single loop approach iteration. By converting the RBDO problem into a deterministic optimization with Kriging model surrogating the constraints, and double loop method can be used to solve it [22]. In [23], a global RBDO method is proposed by surrogating both objective function and LSF with Kriging, and using two strategies to evaluate the optimal solution. Zhang et al. [24] propose a decoupled RBDO method by using double loop Kriging model. Moustapha et al. [25] propose a quantile and Kriging-based RBDO method, where the probabilistic constraints is transformed into the quantiles constraints of the performance criteria. The high-dimensional RBDO problem is solved in [26], where the high-dimensional reliability

analysis method is used to perform reliability analysis, and two strategies are proposed to identify the most probable region of global solution and update the samples for constraints respectively. In [27], the artificial neural network based inverse reliability approach and a small-sample simulation technique are combined with a double loop scheme to solve RBDO. In [28], the comprehensive learning particle swarm optimization is decoupled with GPR model and performed to solve RBDO problems. Yang et al. [29] propose a Kriging-based single loop RBDO method, two criteria are developed to judge the activeness of LSFs and the IMPP is derived to refine the Kriging model. Overall, all the above methods have been proven to be of effective for specific problems, but making better use of the surrogate model information to address RBDO problem is still on the way.

During the past few decades, Bayesian numerical methods based on machine learning, such as Bayesian optimization (BO) [30] and Bayesian cubature (BC) [31], have received explosive developments and special interests in engineering computation, resulting from its many appealing advantages such as global convergence and quantification of numerical error. With the combination of BO and BC, a fully decoupled Bayesian method, called Collaborative and Adaptive Bayesian Optimization (CABO), has been developed for propagating the hybrid uncertainties in our previous work [32, 33], and it shows excellent performance of global convergence and numerical efficiency for even highly nonlinear and multi-modal problems. The aim of this work is then to extend CABO for addressing the RBDO problem. For doing this, we first transform the reliability constrained optimization problem of RBDO into an unconstrained one by the exterior penalty function method, and establish a GPR model in the augmented space of design and random variables for replacing the expensive objective or constraints based on an initial training set. Then, the Bayesian Optimization (BO) is implemented in the design variable space for searching the global optimal design site of the unconstrained optimization problem, and the Bayesian Reliability Analysis (BRA) is implemented in the random variable space for inferring the posterior estimate for the probabilities of failure at the identified point of design variables. The EI and U function are embedded into BO and BRA respectively for generating the next joint training point, where the EI function is evaluated numerically by sampling the posterior GPR model, and by adding it to the training set, the GPR models will be updated. The proposed method has the following appealing features. First, an efficient sampling algorithm for simulating the GPR model is introduced for making it applicable for problems with multiple constraints; second, the equivalent transformation of the constrained problem into a non-constraint one greatly reduces the computational complexity; third, the BO algorithm applied in the design variable space provides guarantee of global convergence; fourth, the BRA applied in the random variable space provides guarantee of convergence for the failure probabilities at the identified optimal points of design variables. The above features of the development are ultimately illustrated and demonstrated with numerical and engineering examples.

2. Problem Statements

Let $\boldsymbol{x} = (x_1, x_2, \cdots, x_n)$ denote n-dimensional independent random input variables whose joint density function is formulated as $f(\boldsymbol{x}|\boldsymbol{\mu})$ with $\boldsymbol{\mu}$ being the mean vector of $\boldsymbol{x}$, and let $\boldsymbol{d} = (d_1, d_2, \cdots, d_m)$ imply the m-dimensional deterministic interval variables. Let $g_i(\boldsymbol{x}, \boldsymbol{d})$ $(i = 1, 2, \cdots, n_c)$ denote a set of n_c limit state functions, each of which represents a failure mode. The objective function of a RBDO problem is denoted

by $J(\boldsymbol{\mu}, \boldsymbol{d})$. With the above notations ready, the RBDO problem is then formulated as:

$$\begin{aligned} &\text{find} && (\boldsymbol{\mu}, \boldsymbol{d}) \\ &\text{minimize} && J(\boldsymbol{\mu}, \boldsymbol{d}) \\ &\text{subjected to:} && \Pr\left(g_i(\boldsymbol{x}, \boldsymbol{d}) < 0\right) < p_{f_i}^*, i = 1, \cdots, n_c \\ & && \boldsymbol{\mu} \in \left[\boldsymbol{\mu}^L, \boldsymbol{\mu}^U\right], \boldsymbol{d} \in \left[\boldsymbol{d}^L, \boldsymbol{d}^U\right] \end{aligned} \tag{1}$$

where $\Pr(\cdot)$ indicates the probabilistic operator, $p_{f_i}^*$ is the threshold of failure probability for the i-th failure mode.

The complexity of the above RBDO problem involves a multidimensional integration with discontinuous integrand for reliability analysis and a multidimensional optimization under complicated constraints. The challenges appear as the LSFs can be highly nonlinear, expensive to evaluate, and the optimization problem can be multi-modal. As has been stated in the introduction, many methods have been developed for solving this RBDO problem, and the surrogate-based RBDO methods have received the most attention due to its high efficiency. In this work, the BO and BRA algorithms are combined to develop a new Bayesian algorithm, called Collaborative and Adaptive Bayesian Optimization (CABO), for searching the global optimal point for the RBDO problem with the least calls of the limit state functions.

3. Collaborative and Adaptive Bayesian Optimization for RBDO

3.1. Reformulation of RBDO as a non-constrained optimization problem

Basically, the CABO method is based on training GPR models for all the expensive-to-evaluate LSFs involved in the RBDO problem in the augmented space of the random and design variables, and then perform non-constrained BO in the marginal space of design variables, and BRA in the marginal space of the random variables. Thus, before the proposition, we need first to reformulate the RBDO problem as a non-constrained one, and then introduce the probabilistic transformation to reformulate the LSFs defined in the augmented space. Generally, there are two ways of treating the constraints for BO, the first strategy is based on designing a novel acquisition function which can incorporate both the expected improvement of objective and the compliance to constraints [34], but this strategy may lose its advantage for problems with multiple constraints. The second strategy is based on first transforming the constrained problem into a non-constrained one based on e.g., Lagrangian relation [35] and penalty function [36], but this may introduce pitfall as it is no longer suitable to approximate the objective function with the stationary GPR model. In this work, the later strategy is utilized, and the pitfall is fixed by an efficient sampling strategy.

Applying the exterior penalty function, the constrained RBDO problem defined by Eq. (1) can be equivalently reformulated as:

$$\begin{aligned} &\text{find} && (\boldsymbol{\mu}, \boldsymbol{d}) \\ &\text{minimize} && \mathcal{F}(\boldsymbol{\mu}, \boldsymbol{d}) = J(\boldsymbol{\mu}, \boldsymbol{d}) + \alpha \left(\sum_{i=1}^{n_c} \left[\max\left(p_{f_i}(\boldsymbol{\mu}, \boldsymbol{d}) - p_{f_i}^*, 0\right)\right]^2 \right), \\ &\text{subjected to:} && \boldsymbol{\mu} \in \left[\boldsymbol{\mu}^L, \boldsymbol{\mu}^U\right], \boldsymbol{d} \in \left[\boldsymbol{d}^L, \boldsymbol{d}^U\right] \end{aligned} \tag{2}$$

with $\alpha > 0$ being the penalty factor, and $\sum_{i=1}^{n_c} \left[\max\left(p_{f_i}(\boldsymbol{\mu}, \boldsymbol{d}) - p_{f_i}^*, 0\right)\right]^2$ being the penalty term. It

should be noted that the penalty factor α is a positive algorithm parameter introduced for making a trade-off between minimization of the objective and compliance to the constraints. Big value of α results in low tolerance of betraying the constraints, but may also results in low convergence rate, and small value of α may lead to less compliance to the constraints. Thus, a trade-off need to be made for specifying the value of α. Based on our experience, setting α as $\alpha = \frac{|10000 \min[J(d)]|}{\min_i \left[p^*_{f_i}\right]}$ is usually a good choice, and is utilized in this work.

As has been stated, the LSFs are approximated by the GPR model within the augmented space of both design variables $(\boldsymbol{\mu}, \boldsymbol{d})$ and the random input variables $\boldsymbol{x}$. However, given the RBDO formulation displayed in Eq. (1), the LSFs are only explicitly dependent on $\boldsymbol{x}$ and $\boldsymbol{d}$, excluding $\boldsymbol{\mu}$. To fill this gap, a probabilistic transformation needs to be implemented before implementing CABO. As the random variables are assumed to be independent of each other, we take the individual x_k as an example. Let $\boldsymbol{u} = (u_1, \cdots, u_n)$ with each element following a standard normal random variable. Let $F_k(x_k)$ denote the cumulative distribution function of x_k, which is assumed to be continuous. Thus, making $\Phi(u_k) = F_k(x_k)$, the inverse transformation can be formulated as $x_k = F_k^{-1}(\Phi(u_k)|\boldsymbol{\mu}_k)$. For the input vector $\boldsymbol{x}$, denote the transformation as $\boldsymbol{x} = T(\boldsymbol{u}|\boldsymbol{\mu})$ for simplicity. Further, denote the joint input variables $\boldsymbol{\omega}$ by $\boldsymbol{\omega} = (\boldsymbol{u}, \boldsymbol{\mu}, \boldsymbol{d})$, then the g_i-function can be reformulated as $\mathcal{G}_i(\boldsymbol{\omega}) = g_i(T(\boldsymbol{u}|\boldsymbol{\mu}), \boldsymbol{d})$, and the failure probability function $p_{f_i}(\boldsymbol{\mu}, \boldsymbol{d})$ can be reformulated as:

$$p_{f_i}(\boldsymbol{\mu}, \boldsymbol{d}) = \Pr(\mathcal{G}_i(\boldsymbol{\omega}) < 0) = \int_{\mathbb{R}^n} I_{F_i}(\boldsymbol{\omega}) \Phi(\boldsymbol{u}) \, \mathrm{d}\boldsymbol{u}, \tag{3}$$

where $I_{F_i}(\boldsymbol{\omega})$ denotes the indicator function of $\mathcal{G}_i(\boldsymbol{\omega})$, and it equals to one if $\mathcal{G}_i(\boldsymbol{\omega}) < 0$, otherwise, it equals to zero. It should be noted that, in case that the design variables do not contain any element of $\boldsymbol{\mu}$, the above probabilistic transformation is not required.

With the above transformation, the dimension of the uncontrained RBDO problem is $n + n + m$, which may turns the original RBDO problem to a high-dimensional one (larger than 30). For this case, one can embed the dimension reduction techniques to the proposed method.

3.2. Basic Principles of CABO

As all requirements are settled, the key steps of CABO for RBDO are conceptually summarized as follows. First, train a GPR model for each g_i-function in the joint space of random and design variables $(\boldsymbol{u}, \boldsymbol{\mu}, \boldsymbol{d})$ based on the training data set $\mathcal{D}_i = \{\boldsymbol{\omega}_k; \mathcal{G}_i(\boldsymbol{\omega}_k)\}_{k=1,\cdots,N_i}$; second, perform BO to infer the most possible minimum of $\mathcal{F}(\boldsymbol{\mu}, \boldsymbol{d})$ in the subspace of $(\boldsymbol{\mu}, \boldsymbol{d})$, and also search the next training site $\left(\boldsymbol{\mu}^+, \boldsymbol{d}^+\right)$, by adding which to the training data, the knowledge on the global minimum point of $\mathcal{F}(\boldsymbol{\mu}, \boldsymbol{d})$ can be improved to the greatest extent; third, implement the adaptive BRA to infer the posterior feature of the failure probability at the next training point $\left(\boldsymbol{\mu}^+, \boldsymbol{d}^+\right)$, and also to search the next accompanied training site $\boldsymbol{u}^+$ which results in the most reduction of the error of estimating the failure probability at the site $\left(\boldsymbol{\mu}^+, \boldsymbol{d}^+\right)$; forth, denote the new training point in the augmented space as $\boldsymbol{\omega}^+ = \left(\boldsymbol{u}^+, \boldsymbol{\mu}^+, \boldsymbol{d}^+\right)$, compute the value of $\mathcal{G}_i(\boldsymbol{\omega}^+)$ by calling the g_i-functions, and add the new joint training point $\{\boldsymbol{\omega}^+; \mathcal{G}_i(\boldsymbol{\omega}^+)\}$ to the training data set $\mathcal{D}_i$, this way to update the GPR mode; at last, repeat the above procedures until the stopping conditions for both BRA and BO are satisfied. With the above procedures, the global optimal point of the design variables is correctly identified by BO in the marginal space $(\boldsymbol{\mu}, \boldsymbol{d})$, and meanwhile, the failure probability values at this global optimal point are estimated in the marginal space of $\boldsymbol{u}$ with desired accuracy. It should be noted that, for each iteration, only in the forth step, each g_i-function need to be computed for one time, thus total number of g_i-function calls equals to the total number of initial raining points plus the number of iteration, making

the CABO method numerically efficient in nature. The conceptual framework of the CABO is shown in Figure 1.

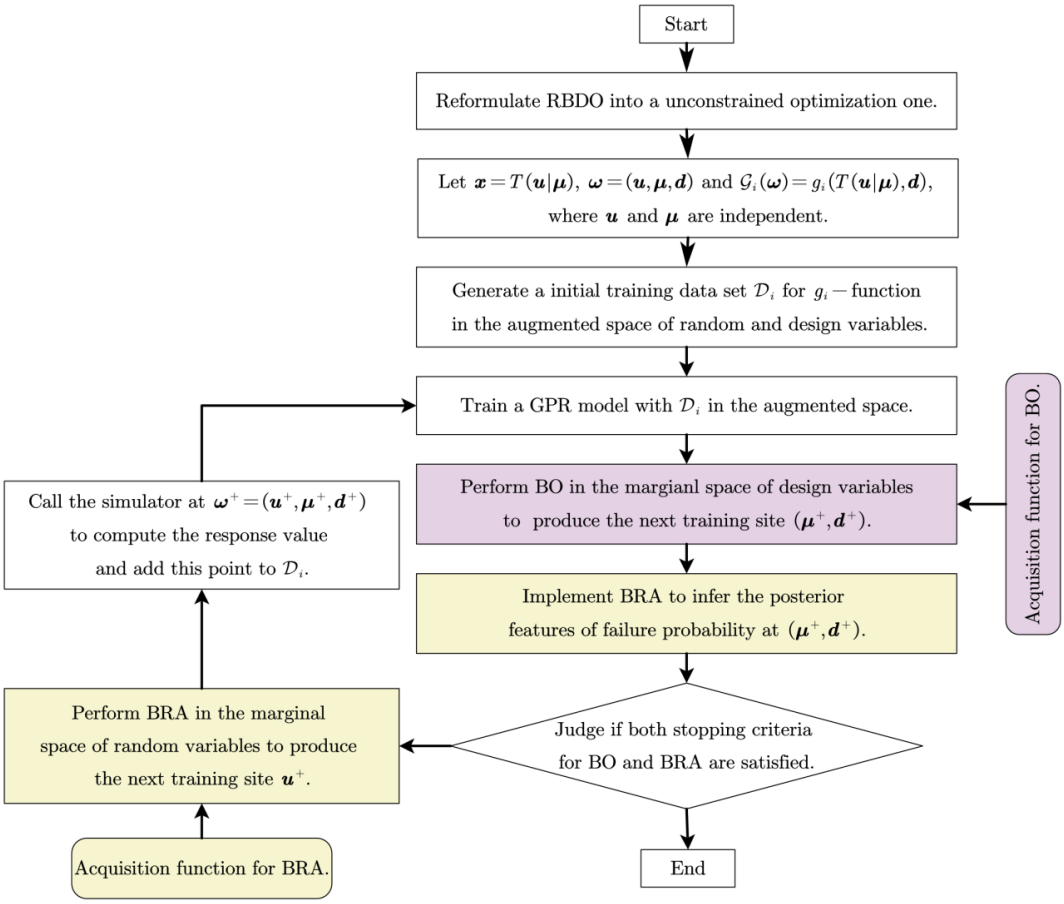

Figure 1: The flowchart of CABO for solving RBDO problem.

As has been revealed by the above description, the key components of the CABO method include: training the GPR models in the augmented space of $\boldsymbol{\omega}$, performing BO in the margianl space of $(\boldsymbol{\mu},\boldsymbol{d})$, and implementing BRA in the marginal space of $\boldsymbol{u}$. Thus, in what follows, these three key components are successively presented.

3.2.1. Gaussian process regression and simulation in augmented space

Without loss of generality, we omit the subscript of $\mathcal{G}_i$, and denote the LSF as $\mathcal{G}(\boldsymbol{\omega})$. Without knowing any information on the value of $\mathcal{G}(\boldsymbol{\omega})$, a GP model, denoted as $\hat{\mathcal{G}}(\boldsymbol{\omega}) \sim \mathcal{GP}(m(\boldsymbol{\omega}), \kappa(\boldsymbol{\omega},\boldsymbol{\omega}'))$, is assumed as a prior for modeling $\mathcal{G}(\boldsymbol{\omega})$, where $m(\boldsymbol{\omega})$ and $\kappa(\boldsymbol{\omega},\boldsymbol{\omega}')$ are the prior mean function and covariance function respectively. One notes that the selection of the functional forms for prior mean and covariance reflects the analysts' prior information on the functional behavior of $\mathcal{G}(\boldsymbol{\omega})$. Generally, the mean function $m(\boldsymbol{\omega})$ can be assumed to be zero, constant or polynomial functions. Thus, the prior mean is formulated as $m(\boldsymbol{\omega}) = \boldsymbol{\beta}^\top \boldsymbol{b}(\boldsymbol{\omega})$, with $\boldsymbol{b}(\boldsymbol{\omega})$ being the vector of functional basis, and $\boldsymbol{\beta}$ being the vector of hyper-parameters. The selection of the prior covariance function $\kappa(\boldsymbol{\omega},\boldsymbol{\omega}')$ (also called kernel function) can be more important

as it reflects the behavior (e.g., smoothness) of the fitted GPR model. One can refer to chapter 4 of Ref. [37] for more details. Without loss of generality, the squared exponential kernel function, which is suitable for modeling any smooth function, is utilized throughout this work. It is formulated as:

$$\kappa\left(\boldsymbol{\omega}, \boldsymbol{\omega}'\right) = \sigma_0^2 \exp\left(-\frac{1}{2}\left(\boldsymbol{\omega} - \boldsymbol{\omega}'\right)\Sigma^{-1}\left(\boldsymbol{\omega} - \boldsymbol{\omega}'\right)^{\mathrm{T}}\right), \tag{4}$$

with σ_0^2 and Σ being the hyper-parameters of the GP model.

Let denote by $\mathcal{D} = (\mathcal{W}, \mathcal{Y})$ the training data set, with $\mathcal{W}$ being a sample matrix of dimension $N_0 \times (2n+m)$ for $\boldsymbol{\omega}$, and $\mathcal{Y}$ is generated by calling the $\mathcal{G}$-function with $\mathcal{W}$, i.e., $\mathcal{Y} = \mathcal{G}(\mathcal{W})$. Based on the prior Gaussian assumption on $\mathcal{G}(\boldsymbol{w})$, the column vector $\mathcal{Y}$ follows a N_0-dimensional Gaussian distribution. Thus, the likelihood function of $\mathcal{D}$, assumed to be the joint density of $\mathcal{Y}$, is formulated as:

$$\mathcal{L}(\mathcal{D}) = \frac{1}{(2\pi)^{N_0/2}\left|\mathcal{K}\right|^{1/2}} \exp\left(-\frac{1}{2}\left(\mathcal{Y} - m(\mathcal{W})\right)^{\top}\mathcal{K}^{-1}\left(\mathcal{Y} - m(\mathcal{W})\right)\right), \tag{5}$$

where $\mathcal{K}$ refers to the covariance matrix computed at the sample points $\mathcal{W}$, i.e., $\mathcal{K} = \kappa(\mathcal{W}, \mathcal{W})$. The logarithm of the above likelihood function can be formulated as:

$$\log \mathcal{L}(\mathcal{D}) \propto -\frac{1}{2}\left(\mathcal{Y} - m(\mathcal{W})\right)^{\top}\mathcal{K}^{-1}\left(\mathcal{Y} - m(\mathcal{W})\right) - \frac{1}{2}\log\left|\mathcal{K}\right|, \tag{6}$$

where $m(\mathcal{W})$ is dependent on the hyper-parameters $\boldsymbol{\beta}$, and $\mathcal{K}$ is dependent on the hyper-parameters σ_0^2 and Σ. Thus, by maximizing $\log \mathcal{L}(\mathcal{D})$, the values of those hyper-parameters can then be estimated [37]. Then, the posterior mean function, posterior variance function and the posterior covariance function can be formulated as:

$$\mu_y(\boldsymbol{\omega}) = m(\boldsymbol{\omega}) + \kappa(\mathcal{W}, \boldsymbol{\omega})^{\mathrm{T}}\mathcal{K}^{-1}\left(\mathcal{Y} - m(\mathcal{W})\right), \tag{7}$$

$$\sigma_y^2(\boldsymbol{\omega}) = \sigma_0^2 - \kappa(\mathcal{W}, \boldsymbol{\omega})^{\mathrm{T}}\mathcal{K}^{-1}\kappa(\mathcal{W}, \boldsymbol{\omega}), \tag{8}$$

and

$$\mathrm{cov}_y(\boldsymbol{\omega}, \boldsymbol{\omega}') = \kappa(\boldsymbol{\omega}, \boldsymbol{\omega}') - \kappa(\mathcal{W}, \boldsymbol{\omega})^{\mathrm{T}}\mathcal{K}^{-1}\kappa(\mathcal{W}, \boldsymbol{\omega}'), \tag{9}$$

respectively, with $\kappa(\mathcal{W}, \boldsymbol{\omega})$ being a N_0-dimensional column vector. The value of mean function $\mu_y(\boldsymbol{\omega})$ at any unobserved site $\boldsymbol{\omega}$ is the mean predictor of $\mathcal{G}(\boldsymbol{\omega})$, while the posterior variance $\sigma_y^2(\boldsymbol{\omega})$ measures the corresponding prediction uncertainty.

To proceed with CABO, we need to generate a set of random samples, denoted by $\hat{\mathcal{G}}^{(k)}(\boldsymbol{\omega}), k = 1, \cdots, N_g$, for the posterior Gaussian process $\hat{\mathcal{G}}_{\mathcal{D}}(\boldsymbol{\omega})$. Here, an efficient sampling strategy, named as "GPR conditioning sampling scheme", is applied to simulate $\hat{\mathcal{G}}_{\mathcal{D}}(\boldsymbol{\omega})$ [38]. Given an unconditional Gaussian process $\tilde{\mathcal{G}}(\boldsymbol{\omega}) \sim \mathcal{GP}(0, \kappa(\boldsymbol{\omega}, \boldsymbol{\omega}'))$, an auxiliary GP model $\hat{\mathcal{H}}_{\mathcal{D}}(\boldsymbol{\omega})$ is defined as:

$$\hat{\mathcal{H}}_{\mathcal{D}}(\boldsymbol{\omega}) = \mu_y(\boldsymbol{\omega}) - \bar{\mu}_y(\boldsymbol{\omega}) + \tilde{\mathcal{G}}(\boldsymbol{\omega}), \tag{10}$$

with $\bar{\mu}_y(\boldsymbol{\omega})$ being formulated as:

$$\bar{\mu}_y(\boldsymbol{\omega}) = \tilde{\boldsymbol{\beta}}^{\top}\boldsymbol{b}(\boldsymbol{\omega}) + \kappa(\mathcal{W}, \boldsymbol{\omega})^{\mathrm{T}}\mathcal{K}^{-1}\left(\tilde{\mathcal{G}}(\mathcal{W}) - \boldsymbol{B}\tilde{\boldsymbol{\beta}}\right), \tag{11}$$

where $\boldsymbol{B}$ denotes the matrix of the basis functions $\boldsymbol{b}(\boldsymbol{\omega})$ computed at $\mathcal{W}$, and $\tilde{\boldsymbol{\beta}} = \left(B^\top \mathcal{K}^{-1} B\right)^{-1} B^\top \mathcal{K}^{-1} \tilde{\mathcal{G}}(\mathcal{W})$. It can be deduced based on Eq. (10) that, the GP model $\hat{\mathcal{H}}_{\mathcal{D}}(\boldsymbol{\omega})$ and $\hat{\mathcal{G}}_{\mathcal{D}}(\boldsymbol{\omega})$ admit the same probability distribution. Therefore, the samples of $\hat{\mathcal{G}}_{\mathcal{D}}(\boldsymbol{\omega})$ can be obtained by simulating $\hat{\mathcal{H}}_{\mathcal{D}}(\boldsymbol{\omega})$, which is equivalent to simulate the unconditional GP model $\tilde{\mathcal{G}}(\boldsymbol{\omega})$. One can refer to [33] for more details.

Let $\hat{\mathcal{G}}_i(\omega)$ denote the GP model trained for approximating the $\mathcal{G}_i$-function involved in Eq. (2). As revealed by Eq. (3) and Eq. (2), the failure probability functions $p_{f_i}(\boldsymbol{\mu}, \boldsymbol{d})$ for $i = 1, \cdots, n_c$ and the resulting objective function $\mathcal{F}(\boldsymbol{\mu}, \boldsymbol{d})$ are all functions of $\mathcal{G}_i(\boldsymbol{\omega})$. By replacing $\mathcal{G}_i(\boldsymbol{\omega})$ with their GPR surrogates $\hat{\mathcal{G}}_i(\omega)$ in these expressions, the resultant quantities $\hat{\mathcal{P}}_{f_i}(\boldsymbol{\mu}, \boldsymbol{d})$ and $\hat{\mathcal{F}}(\boldsymbol{\mu}, \boldsymbol{d})$ are then (non-Gaussian) stochastic processes over the marginal space of the design variables $(\boldsymbol{\mu}, \boldsymbol{d})$. From the perspective of BO, these stochastic processes provide fruitful information for inferring the global optimum point. However, the non-Gaussianity as well as the unavailability of the distribution types and distribution parameters of these stochastic process models, make it untrivial to implement the BO procedure. Alternatively, we propose to realize the BO inference based on the sampling strategy. Instead of directly sampling from the stochastic processes $\hat{\mathcal{P}}_{f_i}(\boldsymbol{\mu}, \boldsymbol{d})$ and $\hat{\mathcal{F}}(\boldsymbol{\mu}, \boldsymbol{d})$, we propose to first generate functional samples $\hat{\mathcal{G}}_i^{(k)}(\boldsymbol{\omega})$, with $k = 1, 2, \cdots, N_g$, from $\hat{\mathcal{G}}_i(\boldsymbol{\omega})$ using the above-mentioned "GPR conditioning sampling scheme", and then numerically compute the corresponding samples $\hat{\mathcal{P}}_{f_i}^{(k)}(\boldsymbol{\mu}, \boldsymbol{d})$ and $\hat{\mathcal{F}}^{(k)}(\boldsymbol{\mu}, \boldsymbol{d})$ respectively, based on MCS, by replacing $\mathcal{G}_i(\boldsymbol{\omega})$ with $\hat{\mathcal{G}}_i^{(k)}(\boldsymbol{\omega})$. Specifically, based on a set of N_u samples, denoted as $\mathcal{U} = \{\boldsymbol{u}_1; \cdots; \boldsymbol{u}_{N_u}\}$, generated from the n-dimensional independent standard Gaussian distribution, the functional samples $\hat{\mathcal{P}}_{f_i}^{(k)}(\boldsymbol{\mu}, \boldsymbol{d})$ and $\hat{\mathcal{F}}^{(k)}(\boldsymbol{\mu}, \boldsymbol{d})$ are estimated by:

$$\hat{\mathcal{P}}_{f_i}^{(k)}(\boldsymbol{\mu}, \boldsymbol{d}) = \frac{1}{N_u} \sum_{j=1}^{N_u} \left[\hat{\mathcal{G}}_i^{(k)}(\boldsymbol{u}_j, \boldsymbol{\mu}, \boldsymbol{d}) < 0\right] \tag{12}$$

and

$$\hat{\mathcal{F}}^{(k)}(\boldsymbol{\mu}, \boldsymbol{d}) = J(\boldsymbol{\mu}, \boldsymbol{d}) + \alpha \left(\sum_{i=1}^{n_c} \left[\max\left(\hat{\mathcal{P}}_{f_i}^{(k)}(\boldsymbol{\mu}, \boldsymbol{d}) - p_{f_i}^*, 0\right)\right]^2\right), \tag{13}$$

respectively. It should be noted that, the objective function can be assumed to be either a cheap-to-evaluate or an expensive-to-compute deterministic function, for the former case, its value at any point of the design variables can be computed with negligible cost, thus does not need to be approximated by a stochastic process model; while for the latter case, a stochastic process model is required to surrogate it.

Once the samples $\hat{\mathcal{F}}^{(k)}(\boldsymbol{\mu}, \boldsymbol{d})$ are generated, the mean prediction $\mu_{\mathcal{F}}(\boldsymbol{\mu}, \boldsymbol{d})$ of $\hat{\mathcal{F}}(\boldsymbol{\mu}, \boldsymbol{d})$ at any site $(\boldsymbol{\mu}, \boldsymbol{d})$ is estimated by the mean of the functional samples $\hat{\mathcal{F}}^{(k)}(\boldsymbol{\mu}, \boldsymbol{d})$, i.e.,

$$\bar{\mu}_{\mathcal{F}}(\boldsymbol{\mu}, \boldsymbol{d}) = \frac{1}{N_g} \sum_{k=1}^{N_g} \hat{\mathcal{F}}^{(k)}(\boldsymbol{\mu}, \boldsymbol{d}), \tag{14}$$

while, the uncertainty of this mean prediction can be quantified by the corresponding variance of the function samples $\hat{\mathcal{F}}^{(k)}(\boldsymbol{\mu}, \boldsymbol{d})$, i.e.,

$$\bar{\sigma}_F^2(\boldsymbol{\mu}, \boldsymbol{d}) = \frac{1}{N_g - 1} \sum_{k=1}^{N_g} \left[\hat{\mathcal{F}}^{(k)}(\boldsymbol{\mu}, \boldsymbol{d}) - \bar{\mu}_{\mathcal{F}}(\boldsymbol{\mu}, \boldsymbol{d})\right]^2. \tag{15}$$

One should note that, all of the above MCS estimators $\hat{\mathcal{P}}_{f_i}^{(k)}(\boldsymbol{\mu}, \boldsymbol{d})$, $\hat{\mathcal{F}}^{(k)}(\boldsymbol{\mu}, \boldsymbol{d})$, $\bar{\mu}_{\mathcal{F}}(\boldsymbol{\mu}, \boldsymbol{d})$ and $\bar{\sigma}_F^2(\boldsymbol{\mu}, \boldsymbol{d})$ are unbiased, meaning that, when the sample size N_u and N_g approach infinity, these estimators convergence

to their true values.

For illustrating the above sampling strategy, a simple numerical example of RBDO with $J(d) = (d-1)^2$ and $g(x,d) = x(\cos(\pi d)+1)+d$ being the objective and LSF respectively, where x follows a standard normal distribution, d denotes the design variable with support $[0,2]$ and p_f^* is set to be 0.05. Based on "GPR conditioning sampling scheme" and 15 training samples, a GPR model is trained, and then one hundred functional samples of which are generated. According to Eq. (12) and (13), one hundred functional samples for $\hat{\mathcal{F}}(d)$ and $\hat{\mathcal{P}}_f(d)$ are deduced, as shown in Figure 2, together with the true functions $\mathcal{F}(d)$ and $p_f(d)$ for comparison. It is shown that these functional samples show variation, which is adapted from the uncertainty of the GPR model trained by few samples, and with more training samples being added to the training set, this kind of variation will be reduced. Although the probability distributions of $\hat{\mathcal{F}}_y$ and $\hat{\mathcal{P}}_f$ cannot be precisely known, these functional samples do provide sufficient information for performing BO in the subspace of design variables.

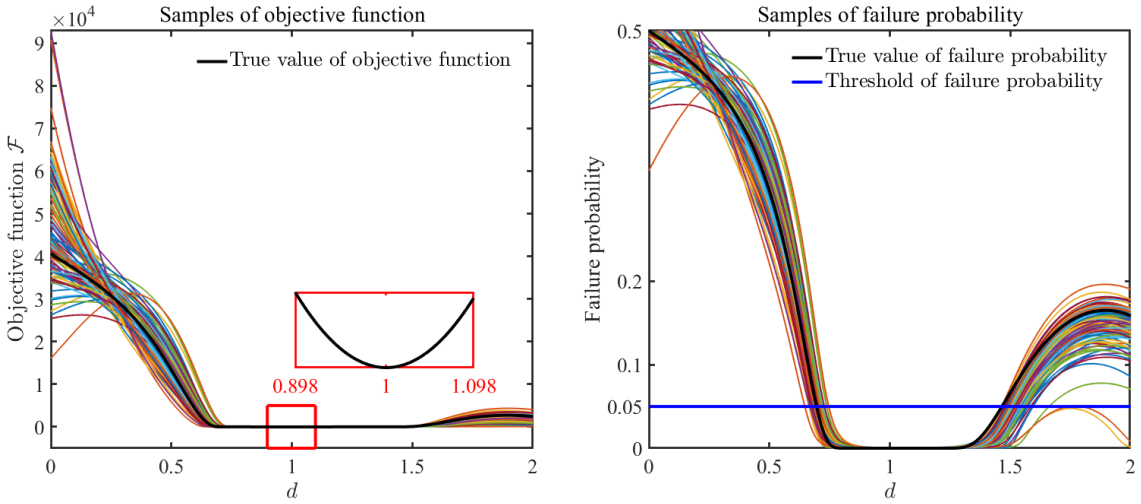

Figure 2: Examples of random samples of objective function (left) and failure probability function (right), which are generated by simulating the GPR model using "GPR conditioning sampling scheme". The true objective function and the failure probability functions are also provided for comparison.

3.2.2. Bayesian optimization in marginal space of design variables

A BO procedure usually involves first training a Bayesian regression model (e.g., a GP model) for approximating the expensive-to-evaluate objective function, and then sequentially producing training points for updating the regression model and for actively inferring the global optimal point with given error tolerance. The performance of a BO procedure is mainly determined by the used acquisition function as it determines the locations at which to observe the objective function. Many acquisition functions have been developed for driving BO in the past few decades, and the well-known ones include the probability of improvement function [39], the expected improvement (EI) function and its many variants [40], the knowledge-gradient function [41], the Upper confidence bound function [42], and the (predictive) entropy search function [43]. The comparison of these acquisition functions for inferring the next design point are summarized in Table 1. With the comprehensive consideration, the EI function is used in this work as it is easy to implement and its global convergence has been demonstrated [44], moreover the UCB function is further used for comparison. Some other acquisition functions can also be adopted for replacing the EI function.

Table 1: Acquisition functions for Bayesian optimization.

Acquisition functions	Illustration	Efficiency
Probability of improvement (PI)	The probability of that the objective function value at $\boldsymbol{x}$ is lower than that of the current best guess	High
Expected improvement (EI)	The expected improvement of the objective function value at $\boldsymbol{x}$ compared to that of the current best guess	High
Knowledge Gradient (KG)	The expected incremental value of a measurement	Low
Upper confidence bound (UCB)	The confidence bound for achieving optimal regret	High
Entropy search (ES)	The expected entropy reduction of the posterior distribution	Low

The classical EI functions usually admit closed-form expressions since the GP model is trained for approximating the objective function. However, as has been stated in subsection 3.2, approximating the objective function $\mathcal{F}(\boldsymbol{\mu}, \boldsymbol{d})$ with a GP model is not appropriate due to its non-smoothness. Instead, an implicit stochastic process model $\hat{\mathcal{F}}(\boldsymbol{\mu}, \boldsymbol{d})$, adapted from the GP models of the LSFs, is used. For this case, the EI function is formulated as:

$$\mathcal{L}^{\mathrm{BO}}(\boldsymbol{\mu}, \boldsymbol{d}) = \mathbb{E}\left(\max\left[\mu_{\mathcal{F}}(\boldsymbol{\mu}^*, \boldsymbol{d}^*) - \hat{\mathcal{F}}(\boldsymbol{\mu}, \boldsymbol{d}), 0\right]\right), \tag{16}$$

where $(\boldsymbol{\mu}^*, \boldsymbol{d}^*)$ denotes the current reference point. Since the distribution types and parameters of $\hat{\mathcal{F}}(\boldsymbol{\mu}, \boldsymbol{d})$ cannot be explicitly known, the EI function defined by Eq. (16) cannot be explicitly formulated in a closed form. Instead, with the samples $\hat{\mathcal{F}}^{(k)}(\boldsymbol{\mu}, \boldsymbol{d}), k = 1, \cdots, N_g$ of $\hat{\mathcal{F}}(\boldsymbol{\mu}, \boldsymbol{d})$, the value of the EI function at a point $(\boldsymbol{\mu}, \boldsymbol{d})$ can be numerically estimated by the following estimator:

$$\hat{\mathcal{L}}^{\mathrm{BO}}(\boldsymbol{\mu}, \boldsymbol{d}) = \frac{1}{N_g}\sum_{k=1}^{N_g} \max\left[\bar{\mu}_{\mathcal{F}}(\boldsymbol{\mu}^*, \boldsymbol{d}^*) - \hat{\mathcal{F}}^{(k)}(\boldsymbol{\mu}, \boldsymbol{d}), 0\right] \tag{17}$$

where mean $\bar{\mu}_{\mathcal{F}}(\boldsymbol{\mu}^*, \boldsymbol{d}^*)$ is computed by Eq. (14). To simplify the calculation, the current reference point $(\boldsymbol{\mu}^*, \boldsymbol{d}^*)$ is obtained by solving the following optimization problem,

$$(\boldsymbol{\mu}^*, \boldsymbol{d}^*) = \arg\min_{(\boldsymbol{\mu}^*, \boldsymbol{d}^*) \in \mathcal{W}} \left[\bar{\mu}_{\mathcal{F}}(\boldsymbol{\mu}, \boldsymbol{d}) + r\bar{\sigma}_{\mathcal{F}}(\boldsymbol{\mu}, \boldsymbol{d})\right] \tag{18}$$

across the observed locations of $(\boldsymbol{\mu}, \boldsymbol{d})$, where r denotes the degree of risk aversion, which is set to be 1 in this work. The term $\max\left[\bar{\mu}_{\mathcal{F}}(\boldsymbol{\mu}^*, \boldsymbol{d}^*) - \hat{\mathcal{F}}(\boldsymbol{\mu}, \boldsymbol{d}), 0\right]$ in Eq. (16) measures the reduction of the objective function at $(\boldsymbol{\mu}, \boldsymbol{d})$ compared to the current best guess $\bar{\mu}_{\mathcal{F}}(\boldsymbol{\mu}^*, \boldsymbol{d}^*)$, and is a random variable with randomness resulted from that of $\hat{\mathcal{F}}(\boldsymbol{\mu}, \boldsymbol{d})$. Therefore, the EI function value at a point $(\boldsymbol{\mu}, \boldsymbol{d})$ measures the expected reduction of the objective function value at $(\boldsymbol{\mu}, \boldsymbol{d})$ compared to that of the reference points. Thus, adding the maximum point of the EI function to the training data set for updating the GPR model, it is expected to improve the knowledge on the true global minimum point of the objective function to the greatest extent. Motivated by this explanation, the next design point is computed by:

$$\left(\boldsymbol{\mu}^+, \boldsymbol{d}^+\right) = \arg\max \hat{\mathcal{L}}^{\mathrm{BO}}(\boldsymbol{\mu}, \boldsymbol{d}). \tag{19}$$

With the estimator in Eq. (17), the EI function has a quasi-analytical expression, and thus its global maximum point can be easily computed with any heuristic algorithms such as the particle swarm algorithm,

without requirement of calling the expensive-to-evaluate LSFs.

If the maximum value of the EI function across the full design variable space is found to be very small, it indicates that no improvement can be obtained, and the global minimum point of the objective function has been correctly identified with high confidence. Thus, the stopping condition for BO can be formulated as:

$$\mathcal{L}^{\mathrm{BO}}\left(\boldsymbol{\mu}^{+}, \boldsymbol{d}^{+}\right) < \Delta^{\mathrm{BO}}, \tag{20}$$

or the normalized one expressed as:

$$\frac{\mathcal{L}^{\mathrm{BO}}\left(\boldsymbol{\mu}^{+}, \boldsymbol{d}^{+}\right)}{\left(\max J\left(\boldsymbol{\mu}_i, \boldsymbol{d}_i\right) - \min J\left(\boldsymbol{\mu}_i, \boldsymbol{d}_i\right)\right)_{\boldsymbol{\mu}_i, \boldsymbol{d}_i \in \mathcal{W}}} < \Delta^{\mathrm{BO}}, \tag{21}$$

where Δ^{BO} denotes the stopping threshold specified in $\left[10^{-3}, 10^{-2}\right]$.

3.2.3. Bayesian reliability analysis in marginal space of random input variables

Once the next design site $\left(\boldsymbol{\mu}^{+}, \boldsymbol{d}^{+}\right)$ in the subspace of design variables is solved by maximizing Eq. (16), to make the corresponding estimate of failure probability $\hat{\mathcal{P}}_{f_i}^{(j)}\left(\boldsymbol{\mu}, \boldsymbol{d}\right)$ more accurate for meeting the given accuracy, the joint design point $\left(\boldsymbol{u}^{+}, \boldsymbol{\mu}^{+}, \boldsymbol{d}^{+}\right)$ is needed for enriching the training data set. Many acquisition functions for searching the design site $\boldsymbol{u}^{+}$ of failure probability estimation in the subspace of random variables have been developed, for example, the U function [45] and the expected integrated error reduction function [46]. The U-function is most commonly used due to its simplicity and effectiveness, thus is used in this work. Given $\left(\boldsymbol{\mu}, \boldsymbol{d}\right)$ being fixed at $\left(\boldsymbol{\mu}^{+}, \boldsymbol{d}^{+}\right)$, the U function for $\hat{\mathcal{G}}_i$ is defined as:

$$\mathrm{U}_i\left(\boldsymbol{u}, \boldsymbol{\mu}^{+}, \boldsymbol{d}^{+}\right) = \frac{\mid \mu_{yi}\left(\boldsymbol{u}, \boldsymbol{\mu}^{+}, \boldsymbol{d}^{+}\right) \mid}{\sigma_{yi}\left(\boldsymbol{u}, \boldsymbol{\mu}^{+}, \boldsymbol{d}^{+}\right)}, \tag{22}$$

The value $\Phi\left(-\mathrm{U}_i\right)$ measures the probability of misjudging the sign of $\hat{\mathcal{G}}_i\left(\boldsymbol{u}, \boldsymbol{\mu}^{+}, \boldsymbol{d}^{+}\right)$ with the posterior mean $\mu_{yi}\left(\boldsymbol{u}, \boldsymbol{\mu}^{+}, \boldsymbol{d}^{+}\right)$. The smaller the value of $U_i\left(\boldsymbol{u}, \boldsymbol{\mu}^{+}, \boldsymbol{d}^{+}\right)$, the higher the probability $\Phi\left(-\mathrm{U}_i\right)$. With the minimum point of U-function being added to $\mathcal{D}_i$, the probability of misjudging the sign of $\mu_{yi}\left(\boldsymbol{u}, \boldsymbol{\mu}^{+}, \boldsymbol{d}^{+}\right)$ will be reduced greatly. Based on this statement, the next design point $\boldsymbol{u}^{+}$ is obtained by choosing the minimum point of U_i-function among the trained GPR models for n_C LSFs in the sample pool $\mathcal{U}$, i.e.,

$$\boldsymbol{u}^{+} = \arg\min_{\boldsymbol{u} \in \mathcal{U}} \min_{i \in (1, \cdots, n_C)} U_i\left(\boldsymbol{u}, \boldsymbol{\mu}^{+}, \boldsymbol{d}^{+}\right). \tag{23}$$

The above adaptive design strategy terminates when the design site $\boldsymbol{u}^{+}$ satisfies the following criterion:

$$\mathrm{COV}_{\mathcal{F}}\left(\boldsymbol{\mu}^{+}, \boldsymbol{d}^{+}\right) = \frac{\bar{\sigma}_{\mathcal{F}}\left(\boldsymbol{\mu}^{+}, \boldsymbol{d}^{+}\right)}{\bar{\mu}_{\mathcal{F}}\left(\boldsymbol{\mu}^{+}, \boldsymbol{d}^{+}\right)} < \Delta^{\mathrm{BRA}}, \tag{24}$$

where $\mathrm{COV}_{\mathcal{F}}$ denotes the Coefficient of Variation (COV) of $\hat{\mathcal{F}}\left(\boldsymbol{\mu}^{+}, \boldsymbol{d}^{+}\right)$, which measures the variation of $\hat{\mathcal{F}}\left(\boldsymbol{\mu}^{+}, \boldsymbol{d}^{+}\right)$ with respect to the mean $\mu_{\mathcal{F}}\left(\boldsymbol{\mu}^{+}, \boldsymbol{d}^{+}\right)$, Δ^{BRA} indicates the termination threshold, which, based on our experience, can be any value in $[0.01, 0.05]$.

Solving Eq. (19) and then Eq. (23), a new design point $\boldsymbol{\omega}^{+} = \left(\boldsymbol{u}^{+}, \boldsymbol{\mu}^{+}, \boldsymbol{d}^{+}\right)$ in the augmented space of design variables and input random variables is obtained. Observing the values of LSFs at this point by computing $y_i^{+} = \mathcal{G}_i\left(\boldsymbol{u}^{+}, \boldsymbol{\mu}^{+}, \boldsymbol{d}^{+}\right)$, the training data $\mathcal{D}_i$ can be enriched, and then based on which, the corresponding GPR model can be updated. The above processes are repeated until the stopping conditions

of Eq. (20) and Eq. (24) are both satisfied. It can be seen from the above procedures, only one simulator call is required for each iteration, indicating the efficiency of the proposed method. And, based on the global convergence of Bayesian optimization, the proposed method is expected to have good performance on global convergence.

3.3. Summary of CABO

With all the above three procedures, i.e., the Bayesian regression fitting and simulation in the augmented space, the BO implemented in the marginal space of the design variables, and the BRA performed in the marginal space of the random variables, the details and pseudocode are then summarized in Algorithm 1. As preliminary treatments, the constrained RBDO problem needs first to be transformed to the equivalent non-constrained optimization problem with target function $\mathcal{F}(\boldsymbol{\mu}, \boldsymbol{d})$ formulated by Eq. (2), and if the design variables involve components of the mean parameters $\boldsymbol{\mu}$ of the random variables $\boldsymbol{x}$, then the nonlinear probabilistic transformation $\boldsymbol{x} = T(\boldsymbol{u}|\boldsymbol{\mu})$ needs to be implemented to transform the LSF $g_i(\boldsymbol{x}, \boldsymbol{d})$ into $\mathcal{G}_i(\boldsymbol{\omega})$ such that the LSFs are depends on all three kinds of parameters, i.e., $\boldsymbol{\omega} = (\boldsymbol{u}, \boldsymbol{\mu}, \boldsymbol{d})$ (see the last paragraph of subsection 3.1).

With the above pre-treatment done, Algorithm 1 starts by generating an initial training data set $\mathcal{D}_i$ of size N_0 for training the GPR model $\hat{\mathcal{G}}_i(\boldsymbol{\omega})$ in the augmented space of $\boldsymbol{\omega}$. Then, with the GPR conditioning sampling scheme presented in subsection 3.2, a set of N_g functional samples, denoted as $\hat{\mathcal{G}}_i^{(k)}(\boldsymbol{\omega})$ with $k = 1, \cdots, N_g$, is generated for each $\hat{\mathcal{G}}_i(\boldsymbol{\omega})$. Based on these functional samples, a set of functional samples for the induced stochastic process of the failure probability function, denoted as $\hat{\mathcal{P}}_{f_i}^{(k)}(\boldsymbol{\mu}, \boldsymbol{d})$ with $k = 1, 2, \cdots, N_g$, can be computed by Eq. (12) using N_u samples of $\boldsymbol{u}$. Further, by substituting $\hat{\mathcal{P}}_{f_i}^{(k)}(\boldsymbol{\mu}, \boldsymbol{d})$ into Eq. (13), a set of functional samples $\hat{\mathcal{F}}^{(k)}(\boldsymbol{\mu}, \boldsymbol{d})$ $(k = 1, 2, \cdots, N_g)$ can also be generated for the induced stochastic process $\hat{\mathcal{F}}(\boldsymbol{\mu}, \boldsymbol{d})$ of the objective function. Using the samples $\hat{\mathcal{F}}^{(k)}(\boldsymbol{\mu}, \boldsymbol{d})$ $(k = 1, 2, \cdots, N_g)$, the BO procedure reported in subsubsection 3.2.2 can be implemented to specify the best guess $(\boldsymbol{\mu}^*, \boldsymbol{d}^*)$ of the global optimal point, the new training point $\left(\boldsymbol{\mu}^+, \boldsymbol{d}^+\right)$ in the marginal space of design variables $(\boldsymbol{\mu}, \boldsymbol{d})$, and also to judge if the stopping condition of Eq. (21) is satisfied. It is then, by fixing $(\boldsymbol{\mu}, \boldsymbol{d})$ at $\left(\boldsymbol{\mu}^+, \boldsymbol{d}^+\right)$, the BRA reported in subsection 3.2.3 is implemented to find the new training point $\boldsymbol{u}^+$ in the marginal space of the random variables $\boldsymbol{u}$, and also to judge the stopping conditioning of Eq. (24) for BRA is satisfied. If the stopping conditions for both BO and BRA are satisfied, the algorithm terminates and produce the global optimal point as $(\boldsymbol{\mu}^*, \boldsymbol{d}^*)$; otherwise, compute the LSF value $\mathcal{G}_i(\boldsymbol{w}^+)$ at the joint training point $\boldsymbol{w}^+ = (\boldsymbol{u}^+, \boldsymbol{\mu}^+, \boldsymbol{d}^+)$, and add the point $(\boldsymbol{w}^+, \mathcal{G}_i(\boldsymbol{w}^+))$ to the training data set $\mathcal{D}_i$ to update the GPR model, and then also repeat the BO and then BRA procedures, until the stopping conditions for both BO and BRA are reached.

Based on the above description, the algorithm parameters of CABO need to be pre-specified include the number N_0 of the initial training sample set, the number N_g of the GPR sample set, the number N_u of the random variable samples, the stopping thresholds Δ^{BO} and Δ^{BRA}, and the penalty factor α. Generally, N_0 can be set to be a small value, e.g., 20, if the prior mean is set to be zero or constant, or set to be $2n+m+1$ if linear prior mean is assumed for the GPR model. The value of N_g is set based on the principle that $\mathrm{COV}_{\mathcal{F}}\left(\boldsymbol{u}^+, \boldsymbol{d}^+\right)$ needs to be less than a threshold. According to some numerical experiences, it is suitable to choose N_g in interval $[1000, 5000]$. The sample size N_u should be set to assure the maximum COV of failure probability sample $\hat{\mathcal{P}}_f^{(k)}$ is less than a given threshold, and it is recommend to set N_u be $100/p_f$, it is this requirement making the proposed method not applicable to extreme small failure probability constraints, e.g., $p_{f_i}^* < 10^{-6}$. This limitation will be fixed in our future work. As has been reported in subsection 3.1, the penalty factor α can be determined adaptive as $\alpha = \frac{|10000 \min[J(d)]|}{\min_i\left[p_{f_i}^*\right]}$. The threshold Δ^{BO} is set to be a

value between 10^{-3} and 10^{-2}, and Δ^{BRA} is set to be a value between 0.01 and 0.05, both of which are based on the error tolerance.

Algorithm 1: CABO method for reliability-based design optimization

Input: Objective function $J(\boldsymbol{\mu}, \boldsymbol{d})$, all of g-function $\mathcal{G}_i(\boldsymbol{w})$ of probabilistic constraints, sample size N_u, N_g, N_0, stopping threshold Δ^{BO}, Δ^{BRA}

Output: The optimal design point $\boldsymbol{\mu}$ and $\boldsymbol{d}$, and the corresponding value of objective function

Generate a set of samples $\mathcal{U}$ of size N_u by random sampling;

Create the initial training set $\mathcal{D}_i$ of the i-the g-function of size N_0 by random sampling. Let $N_{train} = N_0$;

while $(1 = 1)$ **do**

  Train or update the GPR model $\hat{\mathcal{G}}_i(\boldsymbol{\omega})$ based on training data set $\mathcal{D}_i$;

  Generate a set of N_g samples $\hat{\mathcal{G}}_i^{(j)}(\boldsymbol{\omega})$ for $\hat{\mathcal{G}}_i(\boldsymbol{\omega})$ with $j = 1, \cdots, N_g$ by using the GPR conditioning sampling scheme introduced in subsection 3.2;

  Find the current best solution $(\boldsymbol{u}^*, \boldsymbol{d}^*)$ by solving Eq. (18) in $\mathcal{D}$;

  Compute the design site $\left(\boldsymbol{\mu}^+, \boldsymbol{d}^+\right)$ by Eq. (16);

  Compute the design site $\boldsymbol{u}^+$ by minimizing Eq. (22);

  if *both Eq. (20) and Eq. (24) are satisfied* **then**

    break **while-do**;

  else

    Compute the value of $\mathcal{G}_i(\boldsymbol{\omega}^+)$ by calling the simulator, where $\boldsymbol{\omega}^+ = \left(\boldsymbol{u}^+, \boldsymbol{\mu}^+, \boldsymbol{d}^+\right)$, and let $N_{train} = N_{train} + 1$;

    Add $(\boldsymbol{\omega}^+, \mathcal{G}_i(\boldsymbol{\omega}^+))$ to the training data set $\mathcal{D}_i$;

  end

end

It should be noted that, the proposed algorithm can be generally applicable for multi-loop nested coupling problems, as the main idea of which is independent of the distribution type of random variables $\boldsymbol{u}$, the number of probabilistic constraints, and the complexity of objective function.

4. Benchmark study

In this section, two numerical and two engineering examples are used to demonstrate the efficiency and accuracy of the proposed method by comparing it with four RBDO methods, i.e., PMA [7], SORA [9], Quantile-based RBDO [25] and HAK-SLA [18], where the number of g-function calls (NOF) is used to measure the computational efficiencies, while the design point and its corresponding minimum are used to measure the computational accuracy respectively. The results of PMA, SORA and Quantile-based RBDO for all examples are given by using the well-known software platform UQLab developed by Prof. Sudret's team [47], for HAK-SLA, its results are generated by implementing the codes developed by its authors [18]. It should be noted that, the CABO method is charming compared with the above four RBDO methods, as it can provide not only the estimators of design point and optimal value but also their corresponding error measurements, i.e., the coefficient of variation (COV) as given in Eq. (24), which can guarantee estimation precision.

4.1. An highly non-linear illustrative example

We first introduce a widely used numerical example to illustrate the CABO method selected from Ref. [18]. One of the LSFs is highly non-linear, and the RBDO problem is formulated as:

$$\begin{aligned}
&\boldsymbol{\mu}^* = \arg\min J(\boldsymbol{\mu}) = (\mu_1 - 3.7)^2 + (\mu_2 - 4)^2 \\
&\text{s.t.:} f(\boldsymbol{\mu}) = 3 - \mu_1 - \mu_2 < 0 \\
&\quad \mathbb{P}(g_1(\boldsymbol{x}) = x_1 \sin(4x_1) + 1.1x_2 \sin(2x_2) < 0) < \Phi(-2), \\
&\quad \mathbb{P}(g_2(\boldsymbol{x}) = x_1 + x_2 - 3 < 0) < \Phi(-2) \\
&\quad \mu_1 \in [0, 3.7], \mu_2 \in [0, 4]
\end{aligned} \tag{25}$$

where x_i follows a normal distribution $N(\mu_i, 0.1^2)$, $i = 1, 2$, μ_1 and μ_2 are the design variables bounded by interval $[0, 3.7]$ and $[0, 4]$ respectively. The thresholds of failure probability are all set to be $\Phi(-2)$. This example involves only two design variables, and thus allows us to illustrate the details of the learning process of CABO in subspace of design variables. The reference optimal design $\boldsymbol{\mu} = (2.8433, 3.2309)$ and minimum $J(\boldsymbol{\mu}) = 1.3254$ are evaluated by a direct double loop methods, where the failure probability is estimated by MCS with 10^6 samples, and the global optimal solution is solved by particle swarm optimization algorithm.

Before applying CABO to address the above RBDO problem, the initial size of training samples is set to be 15, the stopping thresholds Δ^{BO} and Δ^{BRA} corresponding to BO and BRA respectively are specified as 0.05 and 0.04. With 13 iteration and 13 more training points added to the training set, the CABO method has successfully satisfied the termination conditions, and the detailed processes of CABO in the augmented space of design variables (μ_1, μ_2) are displayed in Figure 3. The reference nephograms of failure probabilities $p_{f_1}(\mu_1, \mu_2)$ and $p_{f_2}(\mu_1, \mu_2)$ are computed by MCS with 10^6 samples, as well as the target failure probability surfaces $p_{f_1}(\mu_1, \mu_2) = \Phi(-2)$ and $p_{f_2}(\mu_1, \mu_2) = \Phi(-2)$. The blue part of the left graph of Figure 3 represents the training details of satisfying the first probability constraint, and from it we can seen that all added training points of (μ_1, μ_2) are located in the feasible domain. The middle graph of Figure 3 displays the training details of approximating the second target failure probability surface near the global optimal point. The right panel illustrates that the added training points are almost all near the constrained optimal point $(2.8433, 3.2309)$ of objective function. The above results demonstrate the effectiveness, global convergence and accuracy of CABO.

The specific results of CABO driven by EI and UCB function, together with SORA, PMA, Quantile-based RBDO and HAK-SLA, as well as the reference value, are given in Table 2. One also can see that, the results of SORA and PMA are the same, this probably because the two methods are all implemented with MPPs. The NOFs required by CABO driven by UCB function and EI function are 33 and 28 respectively, which are the least among these five RBDO methods, where Quantile-based RBDO and HAK-SLA are kriging-based RBDO methods, the NOF required by them are quite larger than that of CABO. Besides, the CABO procedure also provides COV of the objective function $\mathcal{F}(\boldsymbol{\mu})$ estimated at the design point. As shown in Table 2, the COV of $\mathcal{F}(\boldsymbol{\mu})$ is far less than 0.0001, it is because the design point $(2.8219, 3.2437)$ and $(2.8302, 3.2383)$ of CABO are totally in the feasible region determined by the target failure probability surfaces with high credibility. Therefore, the penalty term of all samples of $\hat{\mathcal{F}}(\boldsymbol{\mu})$ given in Eq. (13) at $(2.8219, 3.2437)$ and $(2.8302, 3.2383)$ respectively equals to zero, then all samples have the same value as the original objective function $J(2.8219, 3.2437)$ and $J(2.8302, 3.2383)$, therefore, the COV of $\mathcal{F}(\boldsymbol{\mu})$ approaches to zero. It also can be seen from Table 2, the SORA, PMA and HAK-SLA methods fail to satisfy the failure probability constraint, which is possible because the non-linearity of this problem is too strong for it.

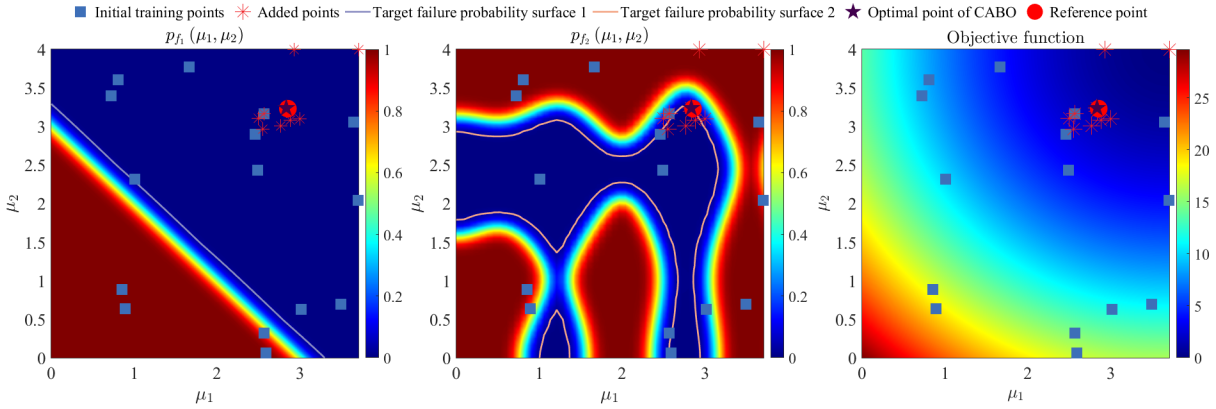

Figure 3: The details of the process for generating adaptive design points of CABO in the numerical example.

Table 2: Results of RBDO problem of the numerical example.

Methods	μ_1	μ_2	minimum	p_{f_1}	p_{f_2}	COV	NOF
Reference value	2.8433	3.2309	1.3254	0.0227	0	–	
SORA	2.8162	3.2770	1.3038	0.0318	0	–	1462
PMA	2.8162	3.2770	1.3038	0.0318	0	–	1497
Quantile-based RBDO	2.8324	3.2384	1.3328	0.0214	0	–	65
HAK-SLA	2.8216	3.2712	1.3027	0.0309	0	–	44
CABO(UCB)	2.8219	3.2437	1.3344	0.0199	0	$\ll 10^{-4}$	15+18=33
CABO(EI)	2.8302	3.2383	1.3367	0.0206	0	$\ll 10^{-4}$	15+13=28

4.2. Middle-dimensional numerical example

For further illustrating the efficiency of CABO method, a middle-dimensional numerical RBDO example is used, which is formulated as:

$$\begin{aligned}
&\boldsymbol{\mu}^* = \arg\min J(\boldsymbol{\mu}) = \mu_1 + \mu_2 + (\mu_3 - 1.5)^2 + \mu_4 + \mu_5 + \mu_6 + \mu_7 + \mu_8 \\
&\qquad\qquad + \mu_9 + \mu_{10} + \mu_{11} + \mu_{12} + \mu_{13} + (\mu_{14} - 1.28)^2 + \mu_{15} \\
&\text{s.t.:} \mathbb{P}\left(g\left(\boldsymbol{x}\right) < 0\right) < 0.005 \\
&\quad g\left(\boldsymbol{x}\right) = \sum_{i=1}^{14} \left[\left(1 - x_i\right)^2 + 100\left(x_{i+1} - x_i^2\right)^2\right] - 650 \\
&\quad \mu_i \in [0, 5, 1.5], i = 1, \cdots, 15
\end{aligned}, \tag{26}$$

where, $x_i \sim N\left(\mu_i, 0.03^2\right)$, their means are denoted by $\boldsymbol{\mu} = (\mu_1, \mu_2, \cdots, \mu_{15})$, and $\mu_i \in [0.5, 1.5], i = 1, \cdots, 15$ denotes the design variables. The LSF is the well known extended Rosenbrock function [48]. It is assumed that the objective function $J\left(\boldsymbol{\mu}\right)$ is easy to compute, and the LSF is expensive-to-estimate and surrogated by GPR model trained in the augmented space of random and interval variables with $15 \times 2 = 30$ dimensional inputs. The reference is solved by a double loop scheme, where the MCS with 10^6 samples is performed to estimate the failure probability, and particle swarm optimization algorithm is applied to search the global optimal point.

The CABO is initialized by setting N_0 to be 75, Δ^{BO} to be 0.001 and Δ^{BRA} to be 0.02 to solve this

middle-dimensional numerical RBDO example. With 13 and 10 more training points adaptively produced by UCB and EI functions of CABO, the stopping conditions for both BO and BRA are reached respectively, and then the results are reported in Table 3, together with the results generated by SORA, PMA, Quantile-based RBDO and HAK-SLA, as well as the reference for comparison. As can be seen from Table 3, Quantile-based RBDO and HAK-SLA methods produce the same results, and do not satisfy the reliability constraints, it is probably because the dimension or non-linearity of g-function for them is too high. The results of SORA are too conservative for this problem, through it satisfies the reliability constraints, the estimator of minimum is too bigger than the reference one. From the view of CABO and PMA, their results are reasonable and acceptable, the required NOFs of CABO are least, therefore, CABO has high efficiency for the expensive-to-evaluate simulator. one can also see that the results of CABO equipped with EI function is better than UCB function demonstrating the superiority of EI for this problem. As shown in Table 3, the COVs of estimator of failure probability of CABO are far less than 0.0001 indicating that the design pint has successfully located at the feasible domain with high accuracy.

Table 3: Results of RBDO problem of the high-dimensional numerical example.

Methods	Design points ($\mu_1 \cdots \mu_{15}$)	minimum	p_f	COV	NOF
Reference	(0.5000, 0.5000, 1.5000, 0.5000, 0.5000, 0.5000, 0.5000, 0.5000, 0.5000, 0.5000, 0.5000, 0.5000, 0.5000, 0.5000, 1.2848, 0.5000)	6.5000	0.005	–	–
SORA	(0.5746, 0.5493, 1.4541, 1.2407, 0.5472, 0.5950, 0.5908, 0.5910, 0.5910, 0.5910, 0.5916, 0.5884, 0.5549, 1.4737, 0.5445)	8.1896	0.0034	–	144936
PMA	(0.5000, 0.5000, 1.5000, 0.5000, 0.5000, 0.5000, 0.5000, 0.5000, 0.5000, 0.5000, 0.5000, 0.5000, 0.5000, 0.5000, 1.2873, 0.5000)	6.5001	0.0045	–	45056
Quantile-based RBDO	(0.5000, 0.5000, 1.4995, 0.5000, 0.5000, 0.5000, 0.5000, 0.5000, 0.5000, 0.5000, 0.5000, 0.5000, 0.5000, 0.5000, 1.2800, 0.5000)	6.5000	0.0065	–	190
HAK-SLA	(0.5000, 0.5000, 1.4995, 0.5000, 0.5000, 0.5000, 0.5000, 0.5000, 0.5000, 0.5000, 0.5000, 0.5000, 0.5000, 0.5000, 1.2800, 0.5000)	6.5000	0.0066	–	112
CABO (UCB)	(0.5000, 0.5000, 1.5000, 0.5000, 0.5000, 0.5000, 0.5000, 0.5000, 0.5000, 0.5000, 0.5000, 0.5000, 0.5000, 0.5000, 1.4107, 0.5000)	6.5171	0.0000	$\ll 10^{-4}$	75+13=88
CABO (EI)	(0.5000, 0.5000, 1.5000, 0.5000, 0.5000, 0.5000, 0.5000, 0.5000, 0.5000, 0.5000, 0.5000, 0.5000, 0.5000, 0.5000, 1.2839, 0.5000)	6.5000	0.0049	$\ll 10^{-4}$	75+10=85

4.3. Journal bearing of air-engine fuel pump

Journal bearing plays an important role in supporting the air-engine fuel pump, its structure is shown in Figure 4, a well-designed bearing can greatly improve the pump's service life. In the practical working environment, geometric dimensioning and cavitation effect possessing aleatory or epistemic uncertainties, will affect the distribution of lubrication film pressure, and further affect lubricating properties of the journal bearing. Therefore, it is urgent to perform RBDO for the journal bearing.

Before applying CABO to address this kind of problem, we should build the lubrication model of journal bearing with the consideration of cavitation. Let θ and y denote the circumferential and axial coordinate of

bearing, h denote the film thickness, which is formulated as

$$h = C\left(1 + \varepsilon\cos\left(\theta\right)\right), \tag{27}$$

where C and ε represent the radial gap and eccentricity ratio of bearing. Let $F_0 = \int_0^h \frac{1}{\eta}dy$, $F_1 = \int_0^h \frac{y}{\eta}dy$, and $F_2 = \int_0^h \frac{y^2}{\eta}dy - \frac{\int_0^h \frac{y}{\eta}dy \int_0^h \frac{y}{\eta}dy}{\int_0^h \frac{1}{\eta}dy}$ with η denoting the viscosity of lubriaction film. Assume that the lubrication film is in-compressible. The pressure distribution $p\left(\theta, y\right)$ of film is governed by the generalized Reynolds equation, which is formulated as

$$\frac{\partial}{\partial x}\left(\frac{\partial p}{\partial x}F_2\right) + \frac{\partial}{\partial z}\left(\frac{\partial p}{\partial z}F_2\right) = \frac{\partial}{\partial x}\left(U\frac{F_1}{F_0}\right), \tag{28}$$

where, $U = \frac{\pi R n_r}{30}$ denotes the speed of shaft with R and n_r denoting its radius and rotate speed respectively. Because of the convergence and divergence region, cavitation always occur. One of most used cavitation boundary conditions is JFO boundary conditions given by the following,

$$p = p_c + g\beta\ln\Theta, \tag{29}$$

where p_c, g, β and $\Theta = \frac{\rho}{\rho_c}$ indicate the cavitation pressure, indicator function of cavitation region, the bulk modulus of film and the density ratio of film's density ρ and cavitation density ρ_c. The pressure distribution of film is solved by integrating the generalized Reynolds equation, JFO boundary conditions simultaneously based on finite difference method in a two dimensional grid.

Assume that, the width B, radius R, radial gap C, rotate speed n_r, initial viscosity η_0 and eccentricity ratio ε are random variables, and the corresponding distribution information are listed in Table 4, together with other deterministic parameters. Let $\boldsymbol{x} = (B, R, C, n, \eta, \varepsilon)$. Fixed the above random variables at their mean, the pressure distribution are displayed in Figure 5. The most important lubricating property of journal bearing is the load capacity, which is computed by the following formula, i.e.,

$$\begin{aligned} F &= \sqrt{F_\xi^2 + F_\eta^2} \\ F_\xi &= -\int_0^B \int_0^{2\pi} p\sin\theta d\theta dz \\ F_\eta &= -\int_0^B \int_0^{2\pi} p\cos\theta d\theta dz \end{aligned}. \tag{30}$$

If the load capacity F is less than a given threshold denoted by $F_{\min}$, the wear will occur and further result in the failure of bearing. Therefore, the LSF of the journal bearing can be formulated as

$$g\left(\boldsymbol{x}\right) = F\left(\boldsymbol{x}\right) - F_{\min}. \tag{31}$$

Let $\boldsymbol{\mu} = (\mu_B, \mu_R, \mu_C)$ represent the design parameters. Our target is to design the geometric size $\boldsymbol{\mu} = (\mu_B, \mu_R, \mu_C)$ of bearing for saving the cost subjected to reliability constraint. The corresponding RBDO

problem can be formulated as

$$\begin{aligned} \boldsymbol{\mu}^* = & \underset{\boldsymbol{\mu}\in[\boldsymbol{\mu}^L,\boldsymbol{\mu}^U]}{\arg\min} \left[\pi R^2 B - \pi\left(R-C\right)^2 B\right] \\ \text{s.t.: } & \mathbb{P}\left[g\left(\boldsymbol{x}\right)<0\right]<0.05 \\ & \left[\boldsymbol{\mu}^L,\boldsymbol{\mu}^U\right] \end{aligned}, \tag{32}$$

where $\boldsymbol{\mu}^L$ is [35e-3, 15e-3,0.058e-3], and $\boldsymbol{\mu}^U$ is [39e-3,17e-3,0.062e-3]. Next, we will apply the proposed method to address the above problem.

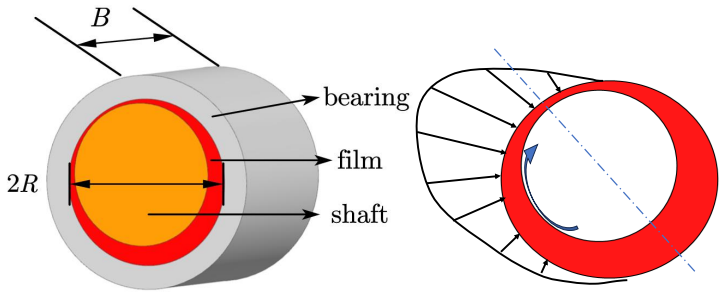

Figure 4: The structure of journal bearing and the pressure distribution of dynamic lubrication.

Table 4: Setting of parameters for the journal bearing.

Parameter	Distribution type	Mean	COV	Value
Bearing's width B (mm)	Normal	$\mu_B \in [35, 39]$	0.005	
Bearing's radius R (mm)	Normal	$\mu_R \in [15, 17]$	0.005	
Radial gap C (mm)	Normal	$\mu_C \in [0.058, 0.062]$	0.005	
Rotate speed n_r $\left(\mathrm{r}\cdot\mathrm{min}^{-1}\right)$	Normal	8000	0.01	
Initial viscosity η_0 (Pa · s)	Normal	9.78×10^{-4}	0.01	
Eccentricity ratio ε	Normal	0.7	0.01	
Cavitation pressure p_c (Pa)				8000
Bulk modulus of film β (Pa)				5×10^8
Density of lubrication film ρ $\left(\mathrm{kg/m}^3\right)$				779
Threshold of load $F_{\min}$ (N)				779

For initializing the CABO algorithm for solving this RBDO problem, N_0 is set to be 15, Δ^{BO} and Δ^{BRA} are set to be 0.001 and 0.03 respectively. With 17 more training points adaptively being added to the training samples set, the termination conditions of CABO are reached. Table 5 displays the results of CABO, together with those generated by SORA, PMA and Quantile-based RBDO. As can be seen from Table 5, the minimums evaluated by SORA, PMA and CABO are basically consistent, as well as the corresponding the design points and failure probabilities, meaning that these three methods generate accurate results. Considering the NOFs and computational time required by the above four RBDO methods, CABO has the least one illustrating its computational efficiency. Moreover, it can be deduced that the failure probability estimated by CABO is accurate as the COV is less than 0.0001, as penalty terms of all samples of $\mathcal{F}\left(\boldsymbol{\mu}\right)$ at the identified design point equal to zero leading the samples to be constant. Based on the above discussion, it can be indicated that the CABO method is more efficient and accurate to design the journal bearing.

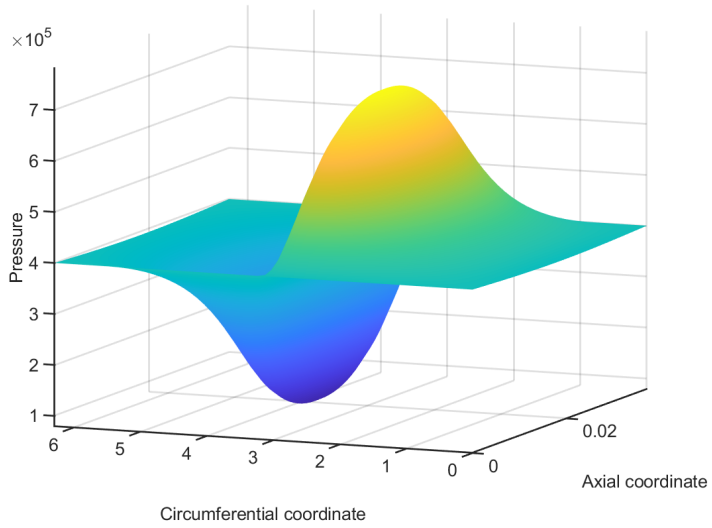

Figure 5: The results of pressure distribution of film by fixing the random parameters at their mean.

Table 5: Results of RBDO problem of the journal bearing

Methods	Design point (μ_B, μ_R, μ_C)	minimum	p_f	COV	NOF	Time (s)
SORA	(35.202e-3,15.001e-3,5.8004e-5)	1.5781e-5	0.0482	–	247	14918.8286
PMA	(35.202e-3,15.001e-3,5.8004e-5)	1.5781e-5	0.0482	–	651	39474.2020
Quantile-based RBDO	(35.694e-3,15.057e-3,5.8428e-5)	1.6121e-5	0.0139	–	60	3648.7634
CABO	(35.234e-3,15.000e-3,5.8000e-5)	1.5794e-5	0.0477	$\ll 10^{-4}$	15+17=32	2651.7990

4.4. Application to a spacecraft attitude control system

The main task of the spacecraft attitude control system is to overcome various internal and external disturbances during flight, guarantee its stability, and ensure the variation of the attitude angle and centroid coordinates meeting the given accuracy. In the process of attitude control system design, it is necessary to consider the uncertainties existing in pneumatic parameters, engine thrust and mass characteristics [49].

By assuming that the influence of inertia of the engine swing tube of a spacecraft can be ignored, the linearized small deviation equations of the pitch channel rigid body motion of is formulated as

$$\begin{aligned} \Delta\dot{\theta} =& (c_2 - c_1)\,\theta + c_1\Delta\varphi + c_3\delta_\varphi + \bar{F}_y \\ \Delta\dot{\omega}_z =& b_2\Delta\theta - b_2\Delta\varphi - b_1\Delta\omega_z - b_3\delta_\varphi + \bar{M}_z, \\ \Delta\dot{\varphi} =& \Delta\omega_z \end{aligned} \tag{33}$$

where $\Delta\theta$, $\Delta\omega_z$, $\Delta\phi$ and δ_ϕ indicate the speed dip, pitch rate, pitch angle, and the equivalent swing angle of tail nozzle respectively, the corresponding rigid body coefficients are given as

$$\begin{aligned} c_1 =& \frac{P + C_L^\alpha qS}{mV}, c_2 = \frac{g\sin\theta}{V}, c_3 = \frac{P}{mV} \\ b_1 =& -\frac{C_{mz}^{\omega z} qSL^2}{J_z V}, b_2 = -\frac{C_{mz}^{\alpha} qSL}{J_z}, b_3 = \frac{C_{mz}^{\delta_z} qSL}{J_z}, \end{aligned} \tag{34}$$

where P, V, q, S, L, m and J_z represent the engine thrust, the spacecraft speed, the dynamic pressure, the

reference area, the reference length, the mass and the moment of inertia respectively, and C_L^{α}, $C_{mz}^{\omega z}$, C_{mz}^{α} and $C_{mz}^{\delta_z}$ denote the pneumatic parameters.

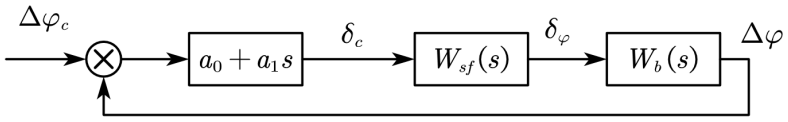

Figure 6: The structure of the pitching channel attitude control system.

Based on the governing equations of motion in Eq. (33), the transfer function of the spacecraft rigid body is formulated as

$$W_b = -\frac{b_3 s + (b_3 c_1 - b_2 c_1 - b_3 c_2)}{s^3 + (b_1 - c_2 + c_1)\, s^2 + (b_1 c_1 - b_1 c_2 + b_2)\, s - b_2 c_2}. \tag{35}$$

The dynamic characters of the servo system of the engine oscillation are approximately replaced by the inertia units, whose transfer function is given by

$$W_{sf} = \frac{1}{T_c s + 1} \tag{36}$$

with T_c denoting the time constant of the servo system. The control methods applies feedback PD control, the corresponding transfer function is formulated as

$$W_c = (a_0 + a_1 s)\,, \tag{37}$$

where a_0 and a_1 represent the static and dynamic gain respectively. Based on the above setting, the transfer function of the open loop of whole control system is formulated as

$$W = W_{sf} W_b W_c. \tag{38}$$

The structure of pitching channel attitude control system is given in Figure 6.

Let $\boldsymbol{x} = \left(C_L^{\alpha}, C_{mz}^{\omega z}, C_{mz}^{\alpha}, C_{mz}^{\delta_z}, a_0, a_1\right)$ and $\boldsymbol{\mu} = (\mu_0, \mu_1)$ denote the random input and design variables, the corresponding distribution information is displayed in Table 6. Assume that the control system will fail when the amplitude margin and phase margin are less than the specified thresholds 15 and 50. The task is to determine the optimal design parameter $\boldsymbol{\mu}$ for maximizing the amplitude margin $L_c\,(\boldsymbol{u}, \boldsymbol{\mu})$ in the conditional of failure probability constraints in the frequency domain. Therefore, the RBDO problem is formulated as

$$\begin{aligned} \boldsymbol{\mu}^* = & \underset{\boldsymbol{\mu} \in [\boldsymbol{\mu}^L, \boldsymbol{\mu}^U]}{\arg\max}\, \mathbb{E}\left[L_c\,(\boldsymbol{u}, \boldsymbol{\mu})\right] \\ \text{s.t.:}\ & \mathbb{P}\left[L_{cd} - L_c\,(\boldsymbol{u}, \boldsymbol{\mu}) < 0\right] < p_{f1}^* = 0.05, \\ & \mathbb{P}\left[\gamma_{cd} - \gamma_c\,(\boldsymbol{u}, \boldsymbol{\mu}) < 0\right] < p_{f2}^* = 0.05 \\ & \boldsymbol{\mu} \in \left[\boldsymbol{\mu}^L, \boldsymbol{\mu}^U\right] \end{aligned} \tag{39}$$

where $\boldsymbol{\mu}^L$ is [0,0], and $\boldsymbol{\mu}^U$ is [3.1,2.0]. The above RBDO problem contains two LSFs and two reliability constraints, and its objective function is also related to the LSFs, which is time-consuming to estimate.

Therefore, SORA, PMA, Quantile-based RBDO and HAK-SLA are inapplicable. Next we use CABO to addressing this RBDO problem.

Table 6: The information of the pneumatic parameter of the spacecraft control system.

Parameters	Distribution type	Means	Std	Ranges
C_L^{α}	Beta	6.4013	0.3201	[5.4411,7.3615]
$C_{mz}^{\omega z}$	Beta	-0.1	0.0050	[-0.1150,-0.0850]
C_{mz}^{α}	Beta	-0.2861	0.0143	[-0.3290,-0.2432]
$C_{mz}^{\delta_z}$	Beta	-0.2792	0.0140	[-0.3211,-0.2373]
a_0	Normal	$\mu_0 \in [0, 3.1]$	0.05	–
a_1	Normal	$\mu_1 \in [0, 2.0]$	0.05	–

Let the initial size of training set, the stopping threshold Δ^{BO} and Δ^{BRA} be 60, 0.05 and 0.04. The CABO method stops by adding 36 more training points to the training samples set, and its results are displayed in Table 7. As can be seen from Table 7, the design point (μ_0, μ_1) estimated by CABO is $(1.5831, 0.5852)$, the maximum of the amplitude margin is 14.3643 and the estimators of failure probabilities p_{f1} and p_{f2} are 0.0468 and 0.0129 less than the given threshold 0.05. The COV is also far less than 0.0001, based on the above discussion, it indicates the high accuracy of the proposed CABO.

Table 7: Results of RBDO problem of the spacecraft control system

Methods	Design point (μ_0, μ_1)	maximum	p_{f1}	p_{f2}	COV	NOF
CABO	$(1.5831, 0.5852)$	14.3643	0.0468	0.0179	$\ll 10^{-4}$	60+36=96

5. Conclusions

For efficiently solving the double-loop RBDO problem for engineering structures simulated with expensive-to-evaluate computational models, a sequential sampling-based Bayesian optimization method, called CABO, has been developed. Using the penalty function method, the constrained RBDO problem is first reformulated as a non-constrained one. Then, by training a GPR model in the joint space of random variables and design variables, the BO and BRA are collaboratively implemented in the two marginal subspace, and this way to produce a joint training point in the augmented space. The above active learning procedure makes it possible for the algorithm to solve the optimization and failure probability estimation in a collaborative and highly efficient way. Thanking to the global convergence of the BO algorithm, the proposed method admits global convergence, and benefiting from the posterior features, the failure probability at the optimal design point can be estimated with desired accuracy. The proposed method is of high accuracy as only one LSF call is required for each iteration.

From the results of the benchmark studies, it is seen that the proposed method exhibit high efficiency, robustness and accuracy, and compared with the several other RBDO methods, it also show superiority. Moreover, the CABO method is applicable to any types of RBDO problem. It should be noted that, the MCS is employed to estimate the failure probability, which will not suitable to rare reliability analysis problem due to the large variation of estimates. Therefore, the advanced MCS procedures, such as subset simulation and line sampling can be integrated into the proposed method, and will be studied in future work.

CRediT authorship contribution statement

Fangqi Hong: Conceptualization, Methodology, Writing - Original draft, Software, Visualization. **Pengfei Wei:** Supervision, Conceptualization, Methodology, Writing - Reviewing and Editing. **Jiangfeng Fu:** Supervision, Writing - Reviewing and Editing. **Michael Beer:** Supervision, Writing - Reviewing and Editing.

Declaration of competing interest

The authors declare that they have no known competing financial interests or personal relationships that could have appeared to influence the work reported in this paper.

Data availability

Data will be made available on request.

Acknowledgment

This work is supported by the National Natural Science Foundation of China under grant number 72171194, and the Sino-German Mobility Programme under grant number M-0175 (2021–2024).

References

[1] W. Yao, X. Chen, W. Luo, M. Van Tooren, J. Guo, Review of uncertainty-based multidisciplinary design optimization methods for aerospace vehicles, Progress in Aerospace Sciences 47 (6) (2011) 450–479.
[2] M. A. Valdebenito, G. I. Schuëller, A survey on approaches for reliability-based optimization, Structural and Multidisciplinary Optimization 42 (2010) 645–663.
[3] T. Chatterjee, S. Chakraborty, R. Chowdhury, A critical review of surrogate assisted robust design optimization, Archives of Computational Methods in Engineering 26 (2019) 245–274.
[4] A. A. Taflanidis, J. L. Beck, Life-cycle cost optimal design of passive dissipative devices, Structural Safety 31 (6) (2009) 508–522.
[5] C. Ling, W. Kuo, M. Xie, An overview of adaptive-surrogate-model-assisted methods for reliability-based design optimization, IEEE Transactions on Reliability (2022).
[6] B. Low, Form, sorm, and spatial modeling in geotechnical engineering, Structural Safety 49 (2014) 56–64.
[7] B. D. Youn, K. K. Choi, An investigation of nonlinearity of reliability-based design optimization approaches, Journal of Mechanical Design 126 (3) (2004) 403–411.
[8] I. Lee, K. Choi, L. Du, D. Gorsich, Inverse analysis method using MPP-based dimension reduction for reliability-based design optimization of nonlinear and multi-dimensional systems, Computer Methods in Applied Mechanics and Engineering 198 (1) (2008) 14–27.
[9] X. Du, W. Chen, Sequential optimization and reliability assessment method for efficient probabilistic design, Journal of Mechanical Design 126 (2) (2004) 225–233.
[10] I. Papaioannou, C. Papadimitriou, D. Straub, Sequential importance sampling for structural reliability analysis, Structural Safety 62 (2016) 66–75.
[11] S.-K. Au, J. L. Beck, Estimation of small failure probabilities in high dimensions by subset simulation, Probabilistic Engineering Mechanics 16 (4) (2001) 263–277.
[12] M. A. Valdebenito, P. Wei, J. Song, M. Beer, M. Broggi, Failure probability estimation of a class of series systems by multidomain line sampling, Reliability Engineering & System Safety 213 (2021) 107673.
[13] K. Cheng, I. Papaioannou, Z. Lu, X. Zhang, Y. Wang, Rare event estimation with sequential directional importance sampling, Structural Safety 100 (2023) 102291.
[14] S. Au, Reliability-based design sensitivity by efficient simulation, Computers & structures 83 (14) (2005) 1048–1061.
[15] X. Yuan, M. A. Valdebenito, B. Zhang, M. G. Faes, M. Beer, Efficient decoupling approach for reliability-based optimization based on augmented line sampling and combination algorithm, Computers & Structures 280 (2023) 107003.
[16] P. Wei, J. Song, S. Bi, M. Broggi, M. Beer, Z. Lu, Z. Yue, Non-intrusive stochastic analysis with parameterized imprecise probability models: II. reliability and rare events analysis, Mechanical Systems and Signal Processing 126 (2019) 227–247.

[17] P. Beaurepaire, H. Jensen, G. Schuëller, M. Valdebenito, Reliability-based optimization using bridge importance sampling, Probabilistic Engineering Mechanics 34 (2013) 48–57.
[18] M. Yang, D. Zhang, C. Jiang, X. Han, Q. Li, A hybrid adaptive Kriging-based single loop approach for complex reliability-based design optimization problems, Reliability Engineering & System Safety 215 (2021) 107736.
[19] Z. Meng, Z. Zhang, D. Zhang, D. Yang, An active learning method combining Kriging and accelerated chaotic single loop approach (AK-ACSLA) for reliability-based design optimization, Computer Methods in Applied Mechanics and Engineering 357 (2019) 112570.
[20] Z. Wu, Z. Chen, G. Chen, X. Li, C. Jiang, X. Gan, L. Gao, S. Wang, A probability feasible region enhanced important boundary sampling method for reliability-based design optimization, Structural and Multidisciplinary Optimization 63 (2021) 341–355.
[21] H. Zhang, Y. Aoues, D. Lemosse, E. S. de Cursi, A single-loop approach with adaptive sampling and surrogate Kriging for reliability-based design optimization, Engineering Optimization 53 (8) (2021) 1450–1466.
[22] Y.-Z. Ma, X.-X. Jin, X.-L. Wu, C. Xu, H.-S. Li, Z.-Z. Zhao, Reliability-based design optimization using adaptive Kriging-A single-loop strategy and a double-loop one, Reliability Engineering & System Safety 237 (2023) 109386.
[23] Y. Pang, X. Lai, S. Zhang, Y. Wang, L. Yang, X. Song, A Kriging-assisted global reliability-based design optimization algorithm with a reliability-constrained expected improvement, Applied Mathematical Modelling 121 (2023) 611–630.
[24] X. Zhang, Z. Lu, K. Cheng, Reliability index function approximation based on adaptive double-loop Kriging for reliability-based design optimization, Reliability Engineering & System Safety 216 (2021) 108020.
[25] M. Moustapha, B. Sudret, J.-M. Bourinet, B. Guillaume, Quantile-based optimization under uncertainties using adaptive Kriging surrogate models, Structural and Multidisciplinary Optimization 54 (2016) 1403–1421.
[26] M. Li, M. Sadoughi, C. Hu, Z. Hu, A. T. Eshghi, S. Lee, High-dimensional reliability-based design optimization involving highly nonlinear constraints and computationally expensive simulations, Journal of Mechanical Design 141 (5) (2019) 051402.
[27] D. Lehkỳ, O. Slowik, D. Novák, Reliability-based design: Artificial neural networks and double-loop reliability-based optimization approaches, Advances in Engineering Software 117 (2018) 123–135.
[28] T. Van Huynh, S. Tangaramvong, B. Do, W. Gao, S. Limkatanyu, Sequential most probable point update combining Gaussian process and comprehensive learning pso for structural reliability-based design optimization, Reliability Engineering & System Safety 235 (2023) 109164.
[29] M. Yang, D. Zhang, F. Wang, X. Han, Efficient local adaptive Kriging approximation method with single-loop strategy for reliability-based design optimization, Computer Methods in Applied Mechanics and Engineering 390 (2022) 114462.
[30] P. I. Frazier, A tutorial on Bayesian optimization, arXiv preprint arXiv:1807.02811 (2018).
[31] P. Wei, X. Zhang, M. Beer, Adaptive experiment design for probabilistic integration, Computer Methods in Applied Mechanics and Engineering 365 (2020) 113035.
[32] P. Wei, F. Hong, K.-K. Phoon, M. Beer, Bounds optimization of model response moments: a twin-engine Bayesian active learning method, Computational Mechanics 67 (5) (2021) 1273–1292.
[33] F. Hong, P. Wei, J. Song, M. A. Valdebenito, M. G. Faes, M. Beer, Collaborative and adaptive Bayesian optimization for bounding variances and probabilities under hybrid uncertainties, Computer Methods in Applied Mechanics and Engineering 417 (2023) 116410.
[34] J. Song, Y. Cui, P. Wei, M. A. Valdebenito, W. Zhang, Constrained Bayesian optimization algorithms for estimating design points in structural reliability analysis, Reliability Engineering & System Safety (2023) 109613.
[35] V. Picheny, R. B. Gramacy, S. Wild, S. Le Digabel, Bayesian optimization under mixed constraints with a slack-variable augmented lagrangian, Advances in Neural Information Processing Systems 29 (2016).
[36] C. Lu, J. A. Paulson, No-regret Bayesian optimization with unknown equality and inequality constraints using exact penalty functions, IFAC-PapersOnLine 55 (7) (2022) 895–902.
[37] C. E. Rasmussen, C. Williams, Gaussian processes for machine learning, vol. 1, MIT press 39 (2006) 40–43.
[38] L. Le Gratiet, C. Cannamela, B. Iooss, A Bayesian approach for global sensitivity analysis of (multifidelity) computer codes, SIAM/ASA Journal on Uncertainty Quantification 2 (1) (2014) 336–363.
[39] J. Wu, X.-Y. Chen, H. Zhang, L.-D. Xiong, H. Lei, S.-H. Deng, Hyperparameter optimization for machine learning models based on Bayesian optimization, Journal of Electronic Science and Technology 17 (1) (2019) 26–40.
[40] D. Zhan, H. Xing, Expected improvement for expensive optimization: a review, Journal of Global Optimization 78 (3) (2020) 507–544.
[41] J. Wu, P. Frazier, The parallel knowledge gradient method for batch Bayesian optimization, Advances in Neural Information Processing Systems 29 (2016).
[42] N. Srinivas, A. Krause, S. M. Kakade, M. Seeger, Gaussian process optimization in the bandit setting: No regret and experimental design, arXiv preprint arXiv:0912.3995 (2009).
[43] J. M. Hernández-Lobato, M. W. Hoffman, Z. Ghahramani, Predictive entropy search for efficient global optimization of black-box functions, Advances in Neural Information Processing Systems 27 (2014).
[44] E. Vazquez, J. Bect, Convergence properties of the expected improvement algorithm with fixed mean and covariance functions, Journal of Statistical Planning and inference 140 (11) (2010) 3088–3095.
[45] B. Echard, N. Gayton, M. Lemaire, AK-MCS: an active learning reliability method combining Kriging and Monte Carlo simulation, Structural Safety 33 (2) (2011) 145–154.
[46] P. Wei, Y. Zheng, J. Fu, Y. Xu, W. Gao, An expected integrated error reduction function for accelerating Bayesian active learning of failure probability, Reliability Engineering & System Safety 231 (2023) 108971.
[47] S. Marelli, B. Sudret, UQLab: A framework for uncertainty quantification in Matlab, in: Proceeding of the 2nd Conference on Vulnerability and Risk Analysis and Management (ICVRAM) and the 6th International Symposium on Uncertainty

Modeling and Analysis (ISUMA), Liverpool, United Kingdom, 2014, pp. 2554–2563.
[48] F. A. Viana, R. T. Haftka, V. Steffen, Multiple surrogates: how cross-validation errors can help us to obtain the best predictor, Structural and Multidisciplinary Optimization 39 (2009) 439–457.
[49] K. Yan, Y. Wu, B. Zhang, Z. Zhong, Probability based method for attitude control system parameters design of space vehicle, Flight Dynamics 39 (1) (2021) 88–94 (translated from Chinese).